Electron-phonon coupling mechanism in two-dimensional graphite and single-wall carbon nanotubes

Ge. G. Samsonidze,[1] E. B. Barros,[1,2] R. Saito,[3] J. Jiang,[3] G. Dresselhaus,[4] and M. S. Dresselhaus[1,5]
[1]*Department of Electrical Engineering and Computer Science, Massachusetts Institute of Technology, Cambridge, Massachusetts 02139-4307, USA*
[2]*Departamento de Física, Universidade Federal do Ceará, Fortaleza 60455-760, Ceará, Brazil*
[3]*Department of Physics, Tohoku University and CREST JST, Aoba, Sendai 980-8578, Japan*
[4]*Francis Bitter Magnet Laboratory, Massachusetts Institute of Technology, Cambridge, Massachusetts 02139-4307, USA*
[5]*Department of Physics, Massachusetts Institute of Technology, Cambridge, Massachusetts 02139-4307, USA*
(Received 19 January 2007; revised manuscript received 6 February 2007; published 19 April 2007)

The electron-phonon coupling in two-dimensional graphite and metallic single-wall carbon nanotubes is analyzed. The highest-frequency phonon mode at the K point in two-dimensional graphite opens a dynamical band gap that induces a Kohn anomaly. Similar effects take place in metallic single-wall carbon nanotubes that undergo Peierls transitions driven by the highest-frequency phonon modes at the Γ and K points. The dynamical band gap induces a nonlinear dependence of the phonon frequencies on the doping level and gives rise to strong anharmonic effects in two-dimensional graphite and metallic single-wall carbon nanotubes.

DOI: 10.1103/PhysRevB.75.155420 PACS number(s): 63.20.Kr, 71.18.+y, 71.70.−d, 73.22.−f

I. INTRODUCTION

Phonon modes of certain symmetries in graphitic materials exhibit a frequency softening, as observed by resonance Raman scattering from *metallic* (metallic armchair and mini-band-gap semiconducting chiral and zigzag) single-wall carbon nanotubes[1] (SWNTs) and by inelastic x-ray scattering from a graphite flake.[2] The frequency softening is attributed to Peierls instabilities in metallic SWNTs (Ref. 3) and to Kohn anomalies in two-dimensional (2D) graphite (a single graphene sheet).[4] The Peierls instability, analogous to the Jahn-Teller effect in molecular systems, occurs when a phonon mode opens a dynamical (oscillating with the phonon frequency) band gap at the Fermi level E_F in a graphene sheet[5] and in metallic SWNTs.[3] The Kohn anomaly occurs when electrons at the Fermi surface screen the phonon mode in a graphene sheet[4] and in metallic SWNTs.[6–9] The two aforementioned phenomena are manifestations of the same underlying electron-phonon coupling mechanism. When a phonon mode opens a dynamical band gap, all the valence electrons lie in states whose energy is lowered, thus reducing the total energy and softening the phonon frequency. On the other hand, the soft phonon mode induces electron scattering at the Fermi surface, which in turn generates charge-density waves, opening a dynamical band gap.

In Sec. II, we derive an analytic expression for the electronic response to the phonon perturbation. In Sec. III, we study the effect of electronic distortion on the phonon frequency. In both sections, we start our consideration with a graphene sheet, and then we extend it to metallic SWNTs. Our approach is based solely on the symmetry of the phonon modes obtained from group theory (GT), and it does not involve the explicit phonon-dispersion relations. The present analysis reveals the *mechanism* of the electron-phonon coupling that is behind Kohn anomalies in a graphene sheet and metallic SWNTs, which is not examined in the previous papers devoted to this subject.

II. PEIERLS INSTABILITY

A graphene sheet is defined by the translation vectors $\mathbf{a}_1$ and $\mathbf{a}_2$ in the two-atom unit cell, as shown in Fig. 1(a) in light gray.[10] The reciprocal-lattice vectors $\mathbf{b}_1$ and $\mathbf{b}_2$ are obtained from $\mathbf{a}_1$ and $\mathbf{a}_2$ following the standard definition $\mathbf{a}_i \cdot \mathbf{b}_j = 2\pi\delta_{ij}$, where δ_{ij} is the Kronecker delta.[10] The first Brillouin zone (BZ) is spanned by $\mathbf{b}_1$ and $\mathbf{b}_2$, as shown in Fig. 1(b) in light gray, where its center and the two inequivalent corners are labeled by the Γ, K, and K' points, respectively.[10] The graphene sheet is a zero-gap semiconductor with the Fermi surface reduced to two points, $\mathbf{k}_F$ and $\mathbf{k}'_F$, which appear, respectively, at the K and K' points.[10] The electrons at the Fermi surface are thus scattered either within the same K or K' point by the phonon modes around the Γ point (intravalley scattering), or between different K and K' points by the phonon modes near the K or K' point (intervalley scattering). Below, we consider the Γ point phonon modes first, and then we turn to the K (K') point phonon modes.

The group of the wave vector at the Γ point (G_Γ) is isomorphic to the point group D_{6h}. The longitudinal and in-

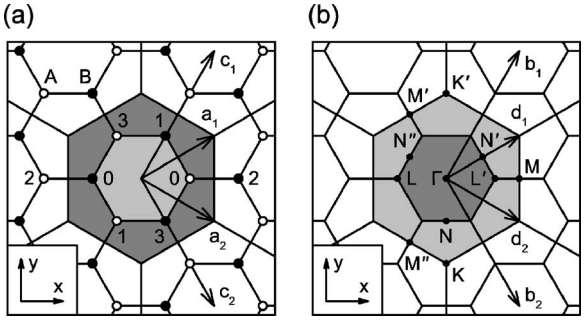

FIG. 1. (a) The two-atom unit cell of the graphene sheet (in light gray) and the six-atom supercell at the K point (in dark gray). (b) The first Brillouin zone (BZ) of the graphene sheet (in light gray) and the triple-folded BZ of the K point supercell (in dark gray).

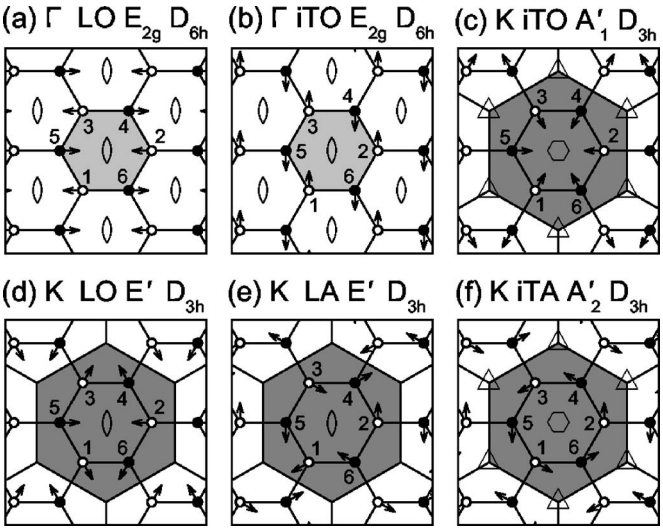

FIG. 2. The arrows show directions of the atomic displacements for the six stationary in-plane optical phonon modes of the graphene sheet at the Γ and K points (Ref. 12). The labels of the phonon modes are explained in the text. The symbols ⬯, △ and ⬡ represent the rotation axes C_2, C_3, and C_6, respectively.

plane transverse optical phonon modes (LO and iTO) belong to the irreducible representation (IR) with E_{2g} symmetry.[11,12] The directions of the atomic displacements specified by IR E_{2g} are shown in Figs. 2(a) and (b), respectively.[12] The Hamiltonian of the graphene sheet distorted by the E_{2g} Γ point phonon mode takes the form

$$H = \begin{pmatrix} H_{AA} & H_{AB} \\ H_{BA} & H_{BB} \end{pmatrix}, \tag{1}$$

where matrix elements H_{AA}, H_{AB}, H_{BA}, and H_{BB} are evaluated within the framework of the nearest-neighbor π-band orthogonal tight-binding model[10] in the linear in u/a approximation, thereafter referred to as a simple tight-binding (STB) model:

$$H_{AA} = E_0 + \lambda \sum_j^3 (\mathbf{u}_{Bj} - \mathbf{u}_{A0}) \cdot (\mathbf{r}_{Bj} - \mathbf{r}_{A0})/a_{CC},$$

$$H_{AB} = \sum_j^3 [t + \alpha(\mathbf{u}_{Bj} - \mathbf{u}_{A0}) \cdot (\mathbf{r}_{Bj} - \mathbf{r}_{A0})/a_{CC}] \times \exp[i\mathbf{k} \cdot (\mathbf{r}_{Bj} - \mathbf{r}_{A0} + \mathbf{u}_{Bj} - \mathbf{u}_{A0})], \tag{2}$$

$H_{BA} = H_{AB}^*$, and $H_{BB} = H_{AA}$. Here, E_0 is the atomic-orbital energy set to zero for our energy scale, $t = -2.56$ eV is the transfer or hopping integral,[13] $\lambda = 39.9$ eV is the on-site electron-phonon coupling (EPC) coefficient,[13] $\alpha = 58.2$ eV/nm is the off-site EPC coefficient,[13] $\mathbf{r}_{Aj}$ and $\mathbf{r}_{Bj}$ are the equilibrium atomic positions shown by the open and solid dots in Fig. 1(a), respectively, $\mathbf{u}_{Aj}$ and $\mathbf{u}_{Bj}$ are the atomic displacements associated with the E_{2g} Γ point phonon mode represented by arrows in Figs. 2(a) and (b), subscript $j = 0, \ldots, 3$ labels the central atom and its three nearest neighbors as illustrated in Fig. 1(a), $a_{CC} = 0.142$ nm is the interatomic distance, and $\mathbf{k}$ is the electron wave vector.

Upon substituting $\mathbf{u}_{Aj}$ and $\mathbf{u}_{Bj}$ from Figs. 2(a) and (b) into Eq. (2) and setting the determinant of Eq. (1) to zero, we find that $\mathbf{k}_F$ ($\mathbf{k}'_F$) oscillates at the phonon frequency with displacement amplitude $\Delta\mathbf{k}_F$ ($\Delta\mathbf{k}'_F$) given by

$$\Delta\mathbf{k}_F = -\Delta\mathbf{k}'_F = -\frac{2\sqrt{3}\alpha u}{ta}\hat{\mathbf{y}} \quad \text{for } \Gamma \text{ LO},$$

$$\Delta\mathbf{k}_F = -\Delta\mathbf{k}'_F = +\frac{2\sqrt{3}\alpha u}{ta}\hat{\mathbf{x}} \quad \text{for } \Gamma \text{ iTO}, \tag{3}$$

around the K (K') point.[3] Here, u is the amplitude of phonon displacements, $a = \sqrt{3}a_{CC} = 0.246$ nm is the lattice constant, and $(\hat{\mathbf{x}}, \hat{\mathbf{y}})$ are the unit vectors shown in the inset of Fig. 1(b). Note that $\Delta\mathbf{k}_F$ and $\Delta\mathbf{k}'_F$ are determined by the off-site EPC coefficient α, since the λ terms in Eq. (2) that are linear in u/a cancel out for the $\mathbf{u}_{Aj}$ and $\mathbf{u}_{Bj}$ vectors shown in Figs. 2(a) and (b).[14]

The group of the wave vector at the K point (G_K) is isomorphic to the point group D_{3h}. Among the longitudinal and in-plane transverse optical and acoustic phonon modes (LO, iTO, LA, and iTA),[15] iTO belongs to IR A'_1 of group D_{3h}, LO and LA to IR E', and iTA to A'_2.[11,12] The directions of the atomic displacements specified by IRs A'_1, E', and A'_2 are shown in Figs. 2(c), (d), (e), and (f), respectively,[12] as are the C_2, C_3, and C_6 rotation axes. Note that the complex traveling phonon modes at the K (K') point only have the C_3 rotation axes, since the group G_K is isomorphic to group D_{3h}.[12] Time-reversal symmetry mixes the complex traveling phonon modes at the K and K' points into the real stationary phonon modes that obey D_{6h} symmetry.[12]

Since the lattice distortions shown in Figs. 2(c), (d), (e), and (f) are incommensurate with the two-atom unit cell, the six-atom supercell must be introduced.[5] The supercell spanned by the translation vectors $\mathbf{c}_1$ and $\mathbf{c}_2$ for which $\mathbf{c}_j \cdot \hat{\mathbf{x}} = \mathbf{a}_j \cdot \hat{\mathbf{x}}$ and $\mathbf{c}_j \cdot \hat{\mathbf{y}} = 3\mathbf{a}_j \cdot \hat{\mathbf{y}}$ ($j = 1, 2$) is shown in Fig. 1(a) in dark gray. The first BZ for the supercell generated by the reciprocal lattice vectors $\mathbf{d}_1$ and $\mathbf{d}_2$ for which $\mathbf{d}_j \cdot \hat{\mathbf{x}} = \mathbf{b}_j \cdot \hat{\mathbf{x}}$ and $\mathbf{d}_j \cdot \hat{\mathbf{y}} = \mathbf{b}_j \cdot \hat{\mathbf{y}}/3$ ($j = 1, 2$) is shown in Fig. 1(b) in dark gray. One can see from Fig. 1(b) that the dark gray hexagon is obtained by cutting the light gray hexagon along six M-L lines and folding it along six L-L lines into one-third of its actual size. The first BZ of the supercell is therefore triple folded, with both the K and K' points ($\mathbf{k}_F$ and $\mathbf{k}'_F$) mapped to the Γ point. The electronic states at the Γ point are therefore fourfold degenerate, but this degeneracy, however, is lifted by the lattice distortions caused by the K point phonon modes. To study the degeneracy-lifting mechanism, we employ GT.

The group of the wave vector G_k (G_Γ or G_K) is isomorphic to the group D_{2h} when the graphene sheet is distorted by the E_{2g} Γ or E' K point phonon modes shown in Figs. 2(c), (d), (e), and (f). The fourfold degenerate electronic state at the Γ point thus consists of the four one-dimensional (1D) IRs of group D_{2h}: two B_{1u} (valence bands) and two B_{2g} (conduction bands). This state therefore splits into two twofold degenerate states $B_{1u} + B_{2g}$ below and above E_F. Such a splitting shifts the band-crossing points $\mathbf{k}_F$ and $\mathbf{k}'_F$ away from the Γ point to states $\mathbf{k}$ and $-\mathbf{k}$, respectively, maintaining the

time-reversal symmetry requirement $\mathbf{k}'_F=-\mathbf{k}_F$. This shift is allowed by GT because the star of a general wave vector $\mathbf{k} \neq 0$ (the set of wave vectors generated from $\mathbf{k}$ by point-group operations) consists of two states, $\mathbf{k}$ and $-\mathbf{k}$. For the E_{2g} Γ point phonon modes, the magnitude of this shift is determined by the off-site EPC coefficient α, according to Eq. (3). In contrast, the magnitude of this shift is governed by the on-site EPC coefficient λ for the E' K point phonon modes, for which $\Delta\mathbf{k}_F$ and $\Delta\mathbf{k}'_F$ are given by Eq. (3) with $\lambda/2$ substituted for α.[14]

The group of the wave vector G_K is isomorphic to the group D_{6h} (C_{6h}) when the graphene sheet is distorted by the A'_1 (A'_2) K point phonon mode shown in Fig. 2(c) [Fig. 2(f)]. The fourfold degenerate electronic state at the Γ point consists of the two 2D IRs of group D_{6h} (C_{6h}): E_{2u} (valence bands) and E_{1g} (conduction bands). This state is therefore not required to split by GT. If it splits, however, a band gap will be opened at the Γ point. Indeed, there are only two inequivalent Fermi points, $\mathbf{k}_F$ and $\mathbf{k}'_F$, while the star of a general wave vector $\mathbf{k} \neq 0$ consists of six states. Thus, $\mathbf{k}_F$ and $\mathbf{k}'_F$ cannot move away from the Γ point.

To check whether the A'_1 (A'_2) K point phonon mode opens a dynamical band gap at the Γ point, we construct the 6×6 STB Hamiltonian at $\mathbf{k}=0$ for the six-atom supercell. Labeling atoms in the supercell as shown by numbers 1–6 in Fig. 2 [atoms 1 to 3 (4 to 6) belong to the A (B) sublattice], the Hamiltonian takes the form of Eq. (1), where H_{AA}, H_{AB}, H_{BA}, and H_{BB} are 3×3 matrices. For an ideal graphene sheet, we have

$$H_{AA}=H_{BB}=\begin{pmatrix} E_0 & 0 & 0 \\ 0 & E_0 & 0 \\ 0 & 0 & E_0 \end{pmatrix},$$

$$H_{AB}=H_{BA}=\begin{pmatrix} t & t & t \\ t & t & t \\ t & t & t \end{pmatrix}. \tag{4}$$

Substituting Eq. (4) into Eq. (1) and setting its determinant to zero yields the following electronic states:

$$E=(E_0+3t,E_0,E_0,E_0,E_0,E_0-3t). \tag{5}$$

The four states $E_j=E_0$ with band index $j=2,3,4,5$ are degenerate, in agreement with the previous discussion.

For the graphene sheet distorted by the A'_1 symmetry K point phonon mode, we construct the STB Hamiltonian considering the atomic displacements shown in Fig. 2(c). Keeping only terms linear in u/a, the λ terms in H_{AA} and H_{BB} cancel out, so that H_{AA} and H_{BB} are the same as in Eq. (4), while H_{AB} and H_{BA} become

$$H_{AB}=H_{BA}=\begin{pmatrix} t+2\alpha u & t-\alpha u & t-\alpha u \\ t-\alpha u & t+2\alpha u & t-\alpha u \\ t-\alpha u & t-\alpha u & t+2\alpha u \end{pmatrix}. \tag{6}$$

Substituting Eqs. (4) and (6) into Eq. (1) and setting its determinant to zero yields the following electronic states:

$$E=(E_0+3t,E_0-3\alpha u,E_0-3\alpha u,E_0+3\alpha u,E_0+3\alpha u,E_0-3t). \tag{7}$$

The A'_1 K point phonon mode thus splits the fourfold degenerate state of Eq. (5), $E_j=E_0$ ($j=2,3,4,5$), into the two twofold degenerate states of Eq. (7), $E_j=E_0-3\alpha u$ ($j=2,3$) and $E_j=E_0+3\alpha u$ ($j=4,5$), opening a dynamical band gap of the following amplitude:

$$E_g=E_4-E_3=6\alpha u \quad \text{for } K\ (K')\ \text{iTO}, \tag{8}$$

which is determined by the off-site EPC coefficient α.[5]

The interatomic distances in the graphene sheet are not affected by the A'_2 symmetry K point phonon mode within the linear in u/a approximation [see in Fig. 2(f)]. Thus, neither λ nor α terms enter the STB Hamiltonian in Eq. (4), and we obtain the fourfold degenerate electronic state at the Γ point described by Eq. (5). However, one of the three interatomic distances in Fig. 2(f) is slightly changed in the second-order series expansion with respect to u/a. Such a deformation opens a dynamical band gap of amplitude $E_g=4\alpha u^2/a$, which is negligible compared to Eq. (8). Thus, the only phonon mode associated with the dynamical band gap in the graphene sheet is the A'_1 K point phonon mode.[5]

For a general phonon wave vector $\mathbf{q}$ away from the Γ and K (K') points, the size of the supercell increases significantly, thereby making the supercell method impractical. We thus implement the linear-response method originally developed within the framework of density-functional perturbation theory[16] and further modified for the extended tight-binding (ETB) model,[9] which operates within the original two-atom unit cell of the graphene sheet. As $\mathbf{q}$ varies from Γ to K (K'), the directions of the atomic displacements $\mathbf{u}_{Aj}$ and $\mathbf{u}_{Bj}$ gradually change from those shown in Fig. 2(a) to the ones in Fig. 2(c). Substituting $\mathbf{u}_{Aj}$ and $\mathbf{u}_{Bj}$ into Eqs. (2) and (6) yields the $\mathbf{q}$-dependent $\Delta\mathbf{k}_F$ ($\Delta\mathbf{k}'_F$) and E_g instead of Eqs. (3) and (8). In the vicinity of the Γ point, we have $qa \ll 1$. Keeping only terms linear in qa yields

$$\Delta\mathbf{k}_F=-\Delta\mathbf{k}'_F=-\frac{2\sqrt{3}\alpha u}{ta}\left(1-\frac{3qa}{2\pi}\right)\hat{\mathbf{y}} \quad \text{for } \Gamma\ \text{LO},$$

$$\Delta\mathbf{k}_F=-\Delta\mathbf{k}'_F=+\frac{2\sqrt{3}\alpha u}{ta}\left(1-\frac{3qa}{2\pi}\right)\hat{\mathbf{x}} \quad \text{for } \Gamma\ \text{iTO}. \tag{9}$$

In the vicinity of the K (K') point, we have $q_K a \ll 1$ ($q_{K'}a \ll 1$). Keeping only terms linear in $q_K a$ ($q_{K'}a$) yields

$$E_g=6\alpha u\left(1-\frac{3q_K a}{2\pi}\right) \quad \text{for } K\ \text{iTO},$$

$$E_g=6\alpha u\left(1-\frac{3q_{K'} a}{2\pi}\right) \quad \text{for } K'\ \text{iTO}, \tag{10}$$

where q_K ($q_{K'}$) is measured from the K (K') point. Thus, the amplitudes $\Delta\mathbf{k}_F$ ($\Delta\mathbf{k}'_F$) and E_g reach their maximum values at the Γ and K (K') points, vanishing halfway between the Γ and K (K') points, according to Eqs. (9) and (10). The detailed derivation of Eqs. (9) and (10) is given in the Appendix.

The same approach can be applied to metallic SWNTs, whose band structure consists of pairs of mirror valence and conduction subbands along the 1D momentum quantization lines in the 2D BZ of the graphene sheet.[10] The A_1' K point phonon mode in metallic SWNTs opens a dynamical band gap or induces oscillations of the mini-band-gap with amplitude given by Eq. (10). The E_{2g} Γ point phonon mode in metallic SWNTs splits into the LO and iTO components involving atomic vibrations in the axial and circumferential directions, respectively. The LO component shifts $\mathbf{k}_F$ and $\mathbf{k}_F'$ perpendicular to the momentum quantization lines, which in turn opens a dynamical band gap or causes oscillations of the mini-band-gap with amplitude given by Eq. (10).[3] The iTO component induces oscillations of $\mathbf{k}_F$ and $\mathbf{k}_F'$ or the band edges along the momentum quantization lines with amplitudes given by Eq. (9).[3]

Let us estimate the numerical values of $\Delta\mathbf{k}_F$ and E_g. Within the second quantization formalism, $u=\xi\sqrt{\rho}$ and $\xi^2=\sqrt{3}a^2\hbar/(4M\omega)$, where u is the amplitude of phonon displacements, ρ is the density of phonon states, M is the mass of a carbon atom, and ω is the phonon frequency. The latter is $\omega(E_{2g})=1582$ cm^{-1} and $\omega(A_1')\approx 1300$ cm^{-1} for the phonon modes of interest.[9,17–19] Integrating ρ over the first BZ gives $\rho=1/A$ per phonon mode, where $A=\sqrt{3}a^2/2=0.052$ nm^2 is an area of the unit cell. On averaging the scaling factor $[1-3qa/(2\pi)]$ in Eqs. (9) and (10) over the first BZ, the effective density of phonon states contributing to $\Delta\mathbf{k}_F$ and E_g is reduced by a factor of $\pi/(18\sqrt{3})=0.1$ for each of the LO E_{2g} Γ, iTO E_{2g} Γ, A_1' K, and A_1' K' point phonon modes. The Bose-Einstein distribution at room temperature $T=300$ K yields $f(E_{2g})=5\times10^{-4}$ and $f(A_1')=2\times10^{-3}$. Putting all the factors together gives $\rho(E_{2g})=10^{-4}$ nm^{-2} and $\rho(A_1')=8\times10^{-4}$ nm^{-2}. Using $\xi(E_{2g})=6.8\times10^{-4}$ nm^2 and $\xi(A_1')=7.5\times10^{-4}$ nm^2, we get $u(E_{2g})=0.7\times10^{-5}$ nm and $u(A_1')=2.1\times10^{-5}$ nm. Substituting these values into Eqs. (3) and (8) yields $|\Delta\mathbf{k}_F|=1.3\times10^{-4}(\Gamma K)$ along the $\hat{\mathbf{y}}$ and $\hat{\mathbf{x}}$ directions for the LO and iTO components of the E_{2g} Γ point phonon mode, and $E_g=10$ meV for the A_1' symmetry K and K' point phonon modes in the graphene sheet. Similarly, $|\Delta\mathbf{k}_F|=1.3\times10^{-4}(\Gamma K)$ for the iTO E_{2g} Γ phonon mode, and $E_g=10$ meV for the LO E_{2g} Γ and A_1' K and K' phonon modes in metallic SWNTs.

III. KOHN ANOMALY

The electronic dispersion relations of an ideal graphene sheet and the graphene sheet distorted by the A_1' K (K') point phonon mode at $T=300$ K are shown in Fig. 3(a) by dashed and solid curves, respectively. The dispersion relations are calculated within the framework of the long-range $\sigma\pi$-band nonorthogonal tight-binding model[13] without making the expansion in a power series in u/a, and thereafter referred to as an ETB model. Considering that the amplitude of the dynamical band gap E_g is less than the thermal energy $T=26$ meV, the former does not affect the transport properties of the graphene sheet at $T=300$ K, though it softens the frequency of the A_1' K (K') point phonon mode. The latter is derived from the equation of motion $M\omega^2u=dE/du$, where E

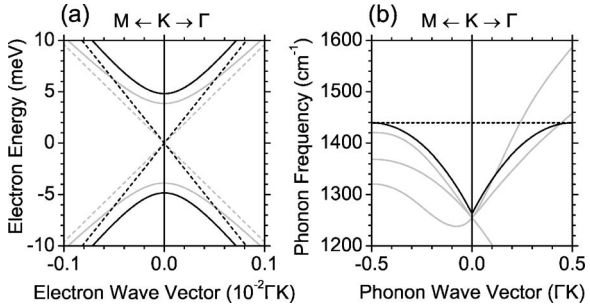

FIG. 3. (a) The electronic dispersion relations of an ideal graphene sheet (dashed curves) and the graphene sheet distorted by the A_1' K point phonon mode at $T=300$ K (solid curves) calculated within the STB (black curves) and ETB (gray curves) models. (b) The phonon-dispersion relations of the graphene sheet calculated within the ETB model (Refs. 9 and 20) at $T=0$ K (gray curves) and from Eq. (15) (solid black curves). The dashed black line shows the leading term in Eq. (15) (with ζ set to zero).

is the total energy of the graphene sheet per carbon atom. In the harmonic approximation, $E=\kappa u^2/2$, where $\kappa=1.02\times10^4$ eV/nm^2 is the effective force constant for the A_1' K (K') point phonon mode. The electronic contribution to E at $T=0$ K is given by the integral of the band energy of the valence electrons over the 2D BZ of the graphene sheet. Formation of the dynamical band gap of width E_g lowers the band energy of the valence π electrons and reduces E. By approximating the valence π-band dispersion around the K (K') point with a cone and integrating it over the 2D BZ of the graphene sheet, we express the change in E at $T=0$ K in the following form:

$$\Delta E = 2\frac{\sqrt{3}a^2}{16\pi^2}\int_0^{2\pi} d\phi \int_0^{k_{\mathrm{BZ}}} kdk[E_v(E_g)-E_v(0)], \quad (11)$$

where a factor of 2 stands for the K and K' points, a circle of radius $k_{\mathrm{BZ}}=2\pi^{1/2}3^{-1/4}a^{-1}$ bounds a half of the 2D BZ,

$$E_v(E_g) = -\sqrt{\frac{3t^2k^2a^2}{4}+E_g^2} \quad (12)$$

is the valence π-band energy when there is a band gap of magnitude E_g given by Eq. (10), while $E_v(0)$ is the case with no phonon perturbation. Upon performing the integration in Eq. (11) and keeping only the leading term in E_g/t, we obtain

$$\Delta E = -\frac{E_g^2}{2\pi^{1/2}3^{1/4}t}. \quad (13)$$

The total energy is then given by

$$E = \left[\kappa - \zeta\left(1-\frac{3\tilde{q}a}{2\pi}\right)^2\right]\frac{u^2}{2}, \quad (14)$$

where $\zeta=-36\alpha^2\pi^{-1/2}3^{-1/4}t^{-1}=2.04\times10^4$ eV/nm^2 and $\tilde{q}=q_K$ ($\tilde{q}=q_{K'}$) for the iTO A_1' K (K') point phonon mode. The phonon frequency is expressed accordingly:

$$\omega = \sqrt{\frac{1}{M}\left[\kappa - \zeta\left(1 - \frac{3\tilde{q}a}{2\pi}\right)^2\right]}. \quad (15)$$

In the vicinity of the K point, $\tilde{q}a \ll 1$, the leading term of Eq. (15) takes the form

$$\omega = \sqrt{\frac{\kappa - \zeta}{M}} + \sqrt{\frac{\zeta}{M}}\frac{3\tilde{q}a}{2\pi}, \quad (16)$$

taking into account that $\zeta \ll \kappa$. The Kohn anomaly thus exhibits a linear dispersion around the K (K') point.[4]

The coefficient ζ in Eq. (14) is calculated analytically by approximating the valence π band with Eq. (12). However, the valence π band starts to deviate from Eq. (12) away from the K (K') point. The valence σ bands also give a nonvanishing contribution to ζ. By performing the numerical integration of the ETB valence $\sigma\pi$-band dispersion distorted by the A_1' K point phonon mode over the 2D BZ of the graphene sheet, we find $\zeta = 0.23 \times 10^4$ eV/nm^2. The phonon-dispersion relations of the graphene sheet calculated within the ETB model[9,20] and those given by Eq. (15) are shown in Fig. 3(b) by gray and black curves, respectively. The leading term of Eq. (15) (with ζ set to zero) is shown in Fig. 3(b) by a dashed line.

In a similar fashion, the E_{2g} Γ point phonon mode in the graphene sheet exhibits a Kohn anomaly[4] driven by the oscillations of $\mathbf{k}_F$ ($\mathbf{k}_F'$) as described by Eq. (9). There is no simple analytical expression for the dispersion of the distorted valence π band around the K (K') point, analogous to Eq. (12) involving the dynamical band gap. We thus perform the numerical integration of the ETB valence $\sigma\pi$-band dispersion distorted by the E_{2g} Γ point phonon mode over the 2D BZ of the graphene sheet. This yields E and ω in the form of Eqs. (14)–(16) with $\kappa = 1.31 \times 10^4$ eV/nm^2 and $\zeta = 0.07 \times 10^4$ eV/nm^2. The Kohn anomaly around the Γ point is indeed seen in the phonon-dispersion relations of the graphene sheet calculated elsewhere.[4,9,18] Note that the oscillations of $\mathbf{k}_F$ ($\mathbf{k}_F'$) only lower E due to the two dimensionality of reciprocal space. As follows from the ETB numerical calculations, the softening of the E_{2g} Γ point phonon mode is dominated by the valence π-band states away from the K (K') point in the 2D BZ of the graphene sheet.

The Kohn anomalies at the Γ and K (K') points in the 2D BZ of the graphene sheet are governed by the electronic contribution to the total energy E, which in turn depends on the doping level. As the Fermi level E_F is moved into the valence or conduction band, the dynamical band gap E_g induced by the A_1' K (K') point phonon mode has less contribution to E, or in other words, ζ in Eqs. (14)–(16) decreases, so that the Kohn anomaly at the K (K') point is smeared out. On the other hand, the oscillations of $\mathbf{k}_F$ ($\mathbf{k}_F'$) induced by the E_{2g} Γ point phonon mode contribute to E regardless of E_F, so that the Kohn anomaly at the Γ point is not affected by E_F. Surely, the Kohn anomalies at the Γ and K (K') points are formed by the valence π-band states away from and close to the K (K') point in the 2D BZ of the graphene sheet, respectively. This is illustrated in Fig. 4(a), where we plot the frequencies of the A_1' K and E_{2g} Γ point phonon modes as a function of the doping level calculated within the ETB framework. While the former frequency increases with changing the doping level, the latter stays constant. However, recent experiments on a graphene sheet show that the frequency of the E_{2g} Γ point phonon mode also increases by changing the doping level.[21] This behavior is attributed to breaking the Born-Oppenheimer approximation.[21–24] The latter is implicit in our ETB calculations, and so the frequency of the E_{2g} Γ point phonon mode in Fig. 4(a) is independent of the doping level. Once the Born-Oppenheimer approximation is broken, the electronic contribution to E and, consequently the frequency of the E_{2g} Γ point phonon mode increase by changing the doping level, as shown elsewhere.[21] Note that a similar increase in the frequency of the A_1' K point phonon mode shown in Fig. 4(a) is induced by the dynamical band gap opening and is not affected by breaking the Born-Oppenheimer approximation.

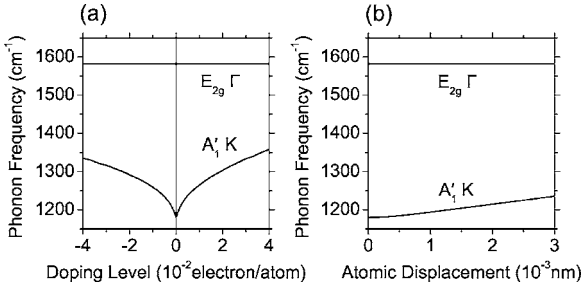

FIG. 4. The frequencies of the E_{2g} Γ and A_1' K point phonon modes in the graphene sheet calculated within the ETB framework as functions of (a) doping level and (b) atomic displacement. The frequency dependence on (a) doping and (b) displacement arises from (a) the dynamical band gap E_g and (b) anharmonicity in the total energy E, which is in turn attributed to E_g.

The dynamical band gap E_g induced by the A_1' K (K') point phonon mode in the graphene sheet gives rise to large anharmonic terms proportional to u^3 and u^4 in the total energy E of Eq. (14). As shown in Fig. 4(b), the frequency of the A_1' K (K') point phonon mode calculated within the ETB framework has a strong dependence on the amplitude of the phonon displacements u. In contrast, the frequency of the E_{2g} Γ point phonon mode is independent of u, according to Fig. 4(b), even though the E_{2g} Γ point phonon mode undergoes a Kohn anomaly. The anharmonicity suggests the importance of the A_1' K point phonon mode for thermal expansion and thermal conductivity in the graphene sheet. A more formal treatment of vibrational anharmonicity in the graphene sheet requires calculation of the phonon-phonon scattering matrix elements, which is beyond the scope of this paper.

In the case of metallic SWNTs, the LO E_{2g} Γ and iTO A_1' K (K') point phonon modes open a dynamical band gap or induce a mini-band-gap oscillation at the K (K') point, according to Sec. II, resulting in Kohn anomalies in the phonon-dispersion relations at the Γ and K (K') points. By analogy with Eq. (11) for the graphene sheet, the variation of the total energy E at $T = 0$ K is obtained by integrating the valence metallic π subbands:

$$\Delta E = \frac{T}{4\pi N} 2 \int_{-\pi/T}^{\pi/T} dk [E_v(E_m + E_g) - E_v(E_m)], \quad (17)$$

where T is the length of the translational unit cell, N is the number of hexagons in the translational unit cell, E_m is the mini-band-gap, E_g is given by Eq. (10), and E_v is the same as Eq. (12). Integration of Eq. (17) yields

$$\Delta E = \frac{tT}{\sqrt{3}\pi Na}\left[- F\left(\frac{E_m + E_g}{t}, \frac{\sqrt{3}\pi a}{2T}\right) + F\left(\frac{E_m}{t}, \frac{\sqrt{3}\pi a}{2T}\right)\right], \quad (18)$$

where we define the following function:

$$F(\Delta, K) = \int_{-K}^{K} \sqrt{x^2 + \Delta^2} dx$$
$$= K\sqrt{K^2 + \Delta^2} + \frac{\Delta^2}{2}[\ln(\sqrt{K^2 + \Delta^2} + K)$$
$$- \ln(\sqrt{K^2 + \Delta^2} - K)]. \quad (19)$$

The mini-band-gap E_m in Eq. (18) is zero for metallic armchair SWNTs and is on the order of room temperature $T=300$ K for mini-band-gap semiconducting chiral and zigzag SWNTs.[25] Upon expanding Eqs. (18) and (19) in a power series in E_g/t up to the second order for mini-band-gap semiconducting chiral and zigzag SWNTs, we find that the total energy is expressed by Eq. (14) with different coefficients κ and ζ for each (n,m) SWNT. For metallic armchair SWNTs, however, the expansion of Eqs. (18) and (19) contains a logarithmic term:

$$\Delta E = \frac{tT}{\sqrt{3}\pi Na}\left(- \frac{E_g^2}{2t^2} + \frac{E_g^2}{t^2} \ln \frac{E_g}{t}\right). \quad (20)$$

The total energy is then given by

$$E = \left(\kappa - \frac{6\sqrt{3}T\alpha^2}{\pi Nat}\left(1 - \frac{3\tilde{q}a}{2\pi}\right)^2 \times \left\{1 - 2\ln\left[\frac{6\alpha u}{t}\left(1 - \frac{3\tilde{q}a}{2\pi}\right)\right]\right\}\right)\frac{u^2}{2}, \quad (21)$$

where $\tilde{q}=q$ and $\tilde{q}=q_K$ ($\tilde{q}=q_{K'}$) for the LO E_{2g} Γ and iTO A_1' K (K') point phonon modes. Once again, the nonlinearity of the electronic dispersion away from the K (K') point and the contribution of the valence nonmetallic σ and π subbands to the total energy influence the numerical coefficients in Eq. (21). The numerical integration of the ETB valence $\sigma\pi$-band dispersion over the 1D BZ of SWNTs yields

$$E = \left\{\kappa + \zeta\left(1 - \frac{3\tilde{q}a}{2\pi}\right)^2 \ln\left[\frac{6\alpha u}{t}\left(1 - \frac{3\tilde{q}a}{2\pi}\right)\right]\right\}\frac{u^2}{2}, \quad (22)$$

where coefficients κ and ζ are different for each (n,m) SWNT. The phonon frequency ω is not simply expressed by the second derivative of Eq. (22) because of its nonanalytic dependence on u. A detailed consideration of the lattice dynamics yields

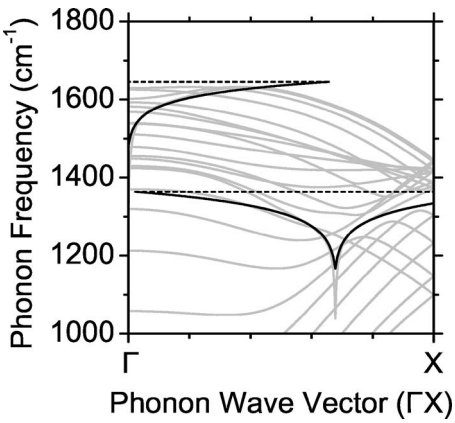

FIG. 5. The phonon-dispersion relations of the (7, 7) SWNT calculated within the ETB model (Refs. 9 and 20) at $T=0$ K (gray curves) and from Eq. (24) (solid black curves). The dashed black line shows the leading term in Eq. (24) (with ζ set to zero).

$$\omega = \sqrt{\frac{1}{M}\left(\kappa + \zeta \ln \frac{3\tilde{q}a}{2\pi}\right)}. \quad (23)$$

Taking into account the inequality $\zeta \ll \kappa$, the leading term of Eq. (23) takes the following form:

$$\omega = \sqrt{\frac{\kappa}{M}} + \frac{1}{2}\sqrt{\frac{\zeta}{M}} \ln \frac{3\tilde{q}a}{2\pi}. \quad (24)$$

The LO E_{2g} Γ and iTO A_1' K (K') point phonon modes thus exhibit a logarithmic divergence[6,8,9,26] for metallic armchair SWNTs, which in turn gives rise to the static Peierls distortions at low T.[7] On the other hand, the iTO E_{2g} Γ point phonon mode that causes oscillations of k_F and k_F' or the band edges along the momentum quantization lines does not induce Kohn anomalies in metallic armchair SWNTs. We omit the analytical integration because of the complexity of the expression for the distorted band structure. However, the numerical integration of the distorted band structure with the displaced $\mathbf{k}_F$ and $\mathbf{k}_F'$ shows that the total energy of the 1D system is independent of the distortion, while the total energy of the 2D system shows a quadratic dependence with the distortion amplitude. The iTO E_{2g} Γ point phonon mode thus exhibits a Kohn anomaly in the graphene sheet but not in metallic armchair SWNTs.

The numerical integration of the ETB valence $\sigma\pi$-band dispersion over the 1D BZ of the (7,7) SWNT yields $\kappa = 0.98 \times 10^4$ eV/nm^2 and $\zeta = 0.27 \times 10^4$ eV/nm^2 for the LO E_{2g} Γ point phonon mode, while $\kappa = 0.76 \times 10^4$ eV/nm^2 and $\zeta = 0.32 \times 10^4$ eV/nm^2 for the iTO A_1' K (K') point phonon mode. The phonon-dispersion relations of the (7,7) SWNT calculated within the ETB model and those given by Eq. (23) with the aforementioned coefficients κ and ζ are shown in Fig. 5.

IV. SUMMARY

In summary, we analyze the electron-phonon coupling in a graphene sheet and in *metallic* SWNTs by combining GT with a tight-binding approach. While most of the phonon

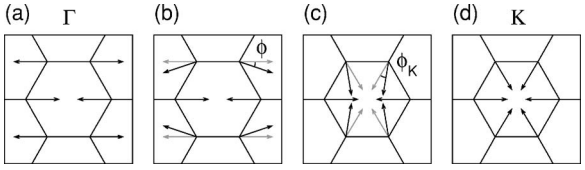

FIG. 6. The arrows show directions of the atomic displacements for the highest-frequency optical phonon mode of the graphene sheet (a) at the Γ point, (b) along the ΓK direction near the Γ point, (c) along the ΓK direction near the K point, and (d) at the K point. Here, (a) and (d) are equivalent to Figs. 2(a) and (c), respectively. The angles indicated in (b) and (c) are given by $\phi=qa/2$ and $\phi_K=q_Ka/2$.

modes in the graphene sheet induce oscillations of the Fermi points in the first BZ, the highest-frequency phonon mode at the K point opens a dynamical band gap at E_F. Both the Fermi point oscillation and the dynamical band gap opening give rise to Kohn anomalies in the phonon spectrum of the graphene sheet, while the dynamical band gap opening also yields strong anharmonic effects. Similar phenomena take place in metallic SWNTs, except that both Kohn anomalies are induced by the dynamical band gaps and not by the Fermi point oscillations. In metallic armchair SWNTs, the dynamical band gap results in a logarithmic divergence of the phonon frequencies and in static Peierls deformations at low T. The dynamical band gap opening discussed in this paper is equivalent to the electron-phonon scattering at the Fermi surface reported in the literature.[4,9]

ACKNOWLEDGMENTS

G.G.S. and E.B.B. thank A. Jorio and L.G. Cançado for helpful discussions about the GT of the K point. The MIT authors acknowledge financial support under NSF Grant No. DMR 04-05538. E.B.B. acknowledges support from CAPES, Brazil. R.S. acknowledges a Grant-in-Aid (No. 16076201) from the Ministry of Education, Culture, Sports, Science and Technology, Japan.

APPENDIX: THE CASE OF A GENERAL PHONON WAVE VECTOR

As the phonon wave vector $\mathbf{q}$ varies from the Γ point to the K (K') point, the directions of the atomic displacements $\mathbf{u}_{A_j}$ and $\mathbf{u}_{B_j}$ gradually change from those shown in Fig. 2(a) to the ones in Fig. 2(c) This gradual change is illustrated in Fig. 6. While Figs. 6(a) and 6(d) are, respectively, identical to Figs. 2(a) and 2(c), Figs. 6(b) and 6(c) correspond to some intermediate wave vectors along the ΓK direction. The directions of $\mathbf{u}_{A_j}$ and $\mathbf{u}_{B_j}$ in Figs. 6(b) and 6(c) are defined by angles $\phi=qa/2$ and $\phi_K=q_Ka/2$, given the rotation of $\mathbf{u}_{A_j}$ and $\mathbf{u}_{B_j}$ from Fig. 6(a) to Fig. 6(d) by angle $2\pi/3$ and the distance of $4\pi/(3a)$ between the Γ and K points.

The Hamiltonian of the graphene sheet distorted by the phonon mode in the vicinity of the Γ point is obtained upon substituting the atomic displacements $\mathbf{u}_{A_j}$ and $\mathbf{u}_{B_j}$ shown in Fig. 6(b) into Eq. (2):

$$H_{AA} = E_0 + \lambda\left\{2u - 2\left[\frac{1}{2} + \cos\left(\frac{\pi}{3} - \phi\right)\right]u\right\},$$

$$H_{AB} = [t + 2\alpha u]\exp[ik_x(a_{CC} + 2u)] + 2\left[t - \alpha\left(\frac{1}{2} + \cos\left(\frac{\pi}{3} - \phi\right)\right)u\right]\exp\left[ik_x\left(-\frac{a_{CC}}{2} + 2u\right)\right] \times \cos\left[k_y\left(-\frac{\sqrt{3}a_{CC}}{2} - \phi u\right)\right]. \quad \text{(A1)}$$

In the vicinity of the Γ point, $q \ll 4\pi/(3a)$ and thus $\phi \ll \pi$. Also taking into account the inequality $u \ll a_{CC}$, Eq. (A1) can be linearized:

$$H_{AA} = E_0 - \sqrt{3}\lambda\phi u,$$

$$H_{AB} = [t(1 + 2ik_x u) + 2\alpha u]\exp[ik_x a_{CC}] + 2[t(1 + 2ik_x u) - \alpha u]\exp\left[-i\frac{k_x a_{CC}}{2}\right]\cos\left[\frac{\sqrt{3}k_y a_{CC}}{2}\right] + 2t\phi k_y u \exp\left[-i\frac{k_x a_{CC}}{2}\right]\sin\left[\frac{\sqrt{3}k_y a_{CC}}{2}\right]. \quad \text{(A2)}$$

Upon substituting Eq. (A2) into Eq. (1) and setting its determinant to zero, we find the Fermi point near the K point in the form $k_{Fx}=\Delta k_{Fx}$ and $k_{Fy}=-4\pi/(3a)+\Delta k_{Fy}$, where Δk_{Fx} and Δk_{Fy} are given by Eq. (9).

In a similar fashion, the 6×6 Hamiltonian of the graphene sheet distorted by the phonon mode in the vicinity of the K (K') point is constructed using the atomic displacements $\mathbf{u}_{A_j}$ and $\mathbf{u}_{B_j}$ shown in Fig. 6(c). To derive the magnitude of the dynamical band gap, it is essential to consider the 6×6 Hamiltonian at $\mathbf{k}=0$, by analogy with Eqs. (4) and (6). The 6×6 Hamiltonian at $\mathbf{k}=0$ can be linearized with respect to $\phi_K \ll \pi$ and $u \ll a_{CC}$ in the same way as Eq. (A2). Finally, we obtain

$$H_{AA} = H_{BB} = \begin{pmatrix} E_0 + \lambda\frac{\sqrt{3}}{2}\phi_K u & 0 & 0 \\ 0 & E_0 - \lambda\sqrt{3}\phi_K u & 0 \\ 0 & 0 & E_0 + \lambda\frac{\sqrt{3}}{2}\phi_K u \end{pmatrix},$$

$$H_{AB} = H_{BA} = \begin{pmatrix} t + 2\alpha u & t - \alpha\left(1 + \frac{\sqrt{3}}{2}\phi_K\right)u & t - \alpha(1 - \sqrt{3}\phi_K)u \\ t - \alpha\left(1 + \frac{\sqrt{3}}{2}\phi_K\right)u & t + 2\alpha u & t - \alpha\left(1 + \frac{\sqrt{3}}{2}\phi_K\right)u \\ t - \alpha(1 - \sqrt{3}\phi_K)u & t - \alpha\left(1 + \frac{\sqrt{3}}{2}\phi_K\right)u & t + 2\alpha u \end{pmatrix}. \quad \text{(A3)}$$

Upon setting the determinant of the Hamiltonian given by Eq. (A3) to zero, we find the magnitude of the dynamical band gap in the form of Eq. (10).

It should be pointed out that the directions of the atomic displacements in Figs. 6(b) and 6(c) are rotated by an integer number of angles ϕ and $2\pi/3 - \phi_K$, respectively, when moving to different unit cells in the graphene sheet. For these unit cells, the Hamiltonians can be constructed by analogy with Eqs. (A1)–(A3). Upon diagonalizing these Hamiltonians, one obtains $\Delta\mathbf{k}_F$ ($\Delta\mathbf{k}'_F$) and E_g that only differ from Eqs. (9) and (10) in the second order with respect to u/a_{CC}, ϕ/π, and ϕ_K/π, in accordance with the linear-response method.[9,16]

[1] M. A. Pimenta, A. Marucci, S. A. Empedocles, M. G. Bawendi, E. B. Hanlon, A. M. Rao, P. C. Eklund, R. E. Smalley, G. Dresselhaus, and M. S. Dresselhaus, Phys. Rev. B **58**, R16016 (1998).

[2] J. Maultzsch, S. Reich, C. Thomsen, H. Requardt, and P. Ordejon, Phys. Rev. Lett. **92**, 075501 (2004).

[3] O. Dubay, G. Kresse, and H. Kuzmany, Phys. Rev. Lett. **88**, 235506 (2002).

[4] S. Piscanec, M. Lazzeri, F. Mauri, A. C. Ferrari, and J. Robertson, Phys. Rev. Lett. **93**, 185503 (2004).

[5] M. Tommasini, E. D. Donato, C. Castiglioni, and G. Zerbi, Chem. Phys. Lett. **414**, 166 (2005).

[6] K.-P. Bohnen, R. Heid, H. J. Liu, and C. T. Chan, Phys. Rev. Lett. **93**, 245501 (2004).

[7] D. Connétable, G.-M. Rignanese, J.-C. Charlier, and X. Blase, Phys. Rev. Lett. **94**, 015503 (2005).

[8] R. Barnett, E. Demler, and E. Kaxiras, Phys. Rev. B **71**, 035429 (2005).

[9] V. N. Popov and P. Lambin, Phys. Rev. B **73**, 085407 (2006).

[10] R. Saito, G. Dresselhaus, and M. S. Dresselhaus, *Physical Properties of Carbon Nanotubes* (Imperial College Press, London, 1998).

[11] We only consider the in-plane optical phonon modes, since the out-of-plane and acoustic phonon modes are only weakly coupled to π electrons.

[12] C. Mapelli, C. Castiglioni, G. Zerbi, and K. Müllen, Phys. Rev. B **60**, 12710 (1999).

[13] D. Porezag, T. Frauenheim, T. Köhler, G. Seifert, and R. Kaschner, Phys. Rev. B **51**, 12947 (1995).

[14] J. Jiang, R. Saito, Ge. G. Samsonidze, S. G. Chou, A. Jorio, G. Dresselhaus, and M. S. Dresselhaus, Phys. Rev. B **72**, 235408 (2005).

[15] The phonon modes at the K point are labeled as iTO, LO, LA, and iTA to identify the branch of the phonon-dispersion relations at the Γ point from which they arise, even though the transverse and longitudinal (optical and acoustic) components are completely mixed at the K point.

[16] S. Baroni, S. de Gironcoli, A. D. Corso, and P. Giannozzi, Rev. Mod. Phys. **73**, 515 (2001).

[17] L. Wirtz and A. Rubio, Solid State Commun. **131**, 141 (2004).

[18] O. Dubay and G. Kresse, Phys. Rev. B **67**, 035401 (2003).

[19] N. Mounet and N. Marzari, Phys. Rev. B **71**, 205214 (2005).

[20] The ETB model systematically overestimates the frequencies of the in-plane phonon modes by about 11%. The calculated frequencies are thus reduced by a factor of 0.9.

[21] S. Pisana, M. Lazzeri, C. Casiraghi, K. S. Novoselov, A. K. Geim, A. C. Ferrari, and F. Mauri, Nat. Mater. **6**, 198 (2007).

[22] A. H. Castro Neto and F. Guinea, Phys. Rev. B **75**, 045404 (2007).

[23] M. Lazzeri, S. Piscanec, F. Mauri, A. C. Ferrari, and J. Robertson, Phys. Rev. B **73**, 155426 (2006).

[24] M. Lazzeri and F. Mauri, Phys. Rev. Lett. **97**, 266407 (2006).

[25] A. Kleiner and S. Eggert, Phys. Rev. B **63**, 073408 (2001).

[26] S. Piscanec, M. Lazzeri, J. Robertson, A. C. Ferrari, and F. Mauri, Phys. Rev. B **75**, 035427 (2007).